Discrete time quantum walk on the Apollonian network

2013 J. Phys. A: Math. Theor. 46 145102

(http://iopscience.iop.org/1751-8121/46/14/145102)

J. Phys. A: Math. Theor. **46** (2013) 145102 (13pp) doi:10.1088/1751-8113/46/14/145102

Discrete time quantum walk on the Apollonian network

A M C Souza[1] **and R F S Andrade**[2]

[1] Departamento de Física, Universidade Federal de Sergipe 49100-000, São Cristovão, Brazil
[2] Instituto de Física, Universidade Federal da Bahia, 40210-340 Salvador, Brazil

E-mail: randrade@ufba.br

Received 2 January 2013, in final form 25 February 2013
Published 26 March 2013
Online at stacks.iop.org/JPhysA/46/145102

Abstract
This work discusses the discrete time quantum walk (DTQW) on the first five generations of the Apollonian network. This structure is constructed in a geometric recurrent way and is characterized by, among other features, a scale-free distribution of node degrees. The DTQW formalism requires a node-dependent coin operator that, for each node, has as many different output states as that node degree, so that each local coin operator is expressed by the Fourier operator. The DTQW time evolution matrix has a larger rank than that of the network adjacency matrix or the matrix representation of the continuous time quantum walk (CTQW). Results for the time evolution, return time to specific nodes and asymptotic probability of site occupancy are obtained. Such DTQW-specific features are discussed and compared to those obtained for the classical random walk and CTQW on the same lattice.

PACS numbers: 89.75.Hc, 05.60.Gg, 03.67.Ac

(Some figures may appear in colour only in the online journal)

1. Introduction

Quantum walks became a subject of great importance in a large number of areas of physics and other sciences. Since they were proposed by Aharonov *et al* [1], a considerable amount of results and applications have been obtained for two well-investigated versions of the original proposition: the discrete time quantum walk (DTQW) [1] and the continuous time quantum walk (CTQW) [2, 3]. Quantum walks can also be related to classical random walks. It can be shown that the continuous time (classical) random walk (CTRW) and CTQW share a similar algebraic structure. Despite the fact that their resulting dynamics are quite different, the time evolution operators for CTQW and CTRW can be expressed by, respectively, an imaginary or real exponential of suitable energy or probability transition matrices.

Regarding the comparison between discrete and continuous dynamics, DTQW and CTQW may be mapped onto one another in some specific parameter limits. Such conditions have been derived for the linear chain and also for some more complex graphs [4–6]. However, the

unrestricted implementation of DTQW (i.e. outside these limiting conditions) has specificities that hinder a direct comparison to the quoted continuous time walks as well as to the discrete time classical random walk (DTRW) dynamics.

DTQW dynamics are specified by sequences of jumps from node i to node j. Transition matrix elements $m_{ij} = 0$ prohibit such jumps and, in this sense, $m_{ij} = 0$ or $m_{ij} \neq 0$ defines the substrate structure. On the other hand, the hopping probability between i and j depends on $m_{ij} \neq 0$ in a specific, model-dependent way. Therefore, for any walk type describing physical relevant transport processes of mass, charge, energy and information, the setup of the proper matrix elements m_{ij} is the essential model formulation step. However, in contrast to the other three types of quoted walks, DTQW also depends on the fact that the probability of such steps depends on an intrinsic state of the walker, usually termed as a coin (or spin) state. This defines a new dynamic behavior presenting distinct features as compared to those in CTQW, CTRW and DTRW.

In this work, we report an investigation on the DTQW on the Apollonian network (AN) [7]. This interesting structure has been used as a substrate to study both classical [8–10] and quantum [11–14] physical models mainly for two reasons: it has common features with several complex networks found in nature and in social systems [15–17], and it can be constructed in a geometrically exact recursive way. Its exact scale invariance allows for the use of renormalization approaches to obtain recursion maps for the several properties of systems at consecutive generations (say, g and $g+1$) from which exact or high precision numerical results [7] are obtained. Furthermore, the AN has the advantage of sharing the following properties: scale-free [18], small world [19] and hierarchical [20].

Analyses of several physical systems revealed that their properties on complex network substrates may be quite different from similar ones observed on disordered models on Euclidian or even fractal structures [21, 22]. Results for CTQW, CTRW and DTRW on AN have been discussed previously [23, 24]. In the continuous time case, the authors have concentrated on the time evolution of the probability transition between specific pairs of nodes. They stressed several differences between quantum and classical behaviors for ANs up to 43 nodes. In the discrete time case, the focus was on the evaluation of the mean first passage time (MFPT). The authors succeeded in deriving an analytical expression showing that the MFPT increases as a power law of the number of nodes in the network.

The results discussed herein are relevant for quantum information since small-world networks may provide a better setup for quantum state transfer and entanglement production between distant nodes. For example, high-dimensional entangled states are required for distributed quantum computation [25] and one-way quantum computation [26] (creation of cluster states). In this view, an analysis of the DTQW in this class of networks seems to be relevant since it gives us an insight into the odd interplay between the many degrees of freedom of the system.

2. Basic features of ANs

For any specific structure, the transition operators required for the DTQW can be expressed in a matrix form. To write down such a matrix, we take into account the most simple situation of a non-weighted, non-directed network for which the corresponding adjacency matrix (A) is a symmetric assembly of 0s and 1s. For ANs, we obtain generation-g-dependent As, which we indicate as A_g. Since we can number the nodes of a complex network in quite arbitrary ways, A_gs may assume different forms that do not change its physical relevant features as the eigenvalue spectrum.

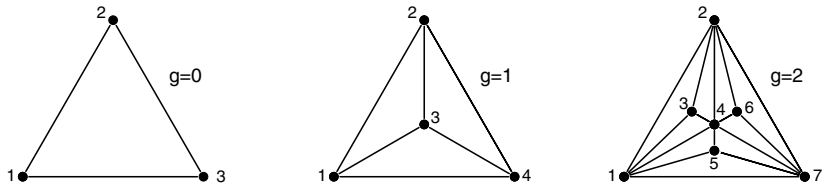

Figure 1. Illustration of the first three generations for the AN with node numbering defined in [11].

We construct generation-dependent ANs by starting with the zeroth generation ($g = 0$), consisting of three nodes that are connected to form an equilateral triangle (see figure 1). The first generation is constructed by adding a node to the interior of this triangle and connecting it to the three existing vertices. Higher order generations are obtained by repeating this two-step procedure: (i) add a node to the interior of each existing triangle; (ii) connect each new node to the three vertices defining the triangle the node has been inserted in.

It is a simple counting matter to obtain expressions for the number of sites N and the number of edges B as a function of g as $N(g) = (3^g + 5)/2$, $B(g) = (3^{g+1} + 3)/2$. These expressions indicate that, in the $g \to \infty$ limit, $B(g)/N(g) \to 3$ and the average node degree $\langle k \rangle \to 6$.

As anticipated in section 1 and pointed out in a series of works, the AN has several properties that are common to other complex networks, among which we may quote the following ones: the distribution $P(k)$ of node degree k is described by a power law with the exponent $\gamma = \ln 3/\ln 2$; the average minimal distance between nodes behaves like $\langle \ell \rangle \sim \log N$; $c(k)$, the clustering coefficient of nodes with degree k, also depends on k as a power law.

Since our results for transition probabilities depend on the precise identification of the nodes on the network, let us explicitly indicate the node enumeration used herein, which is the same as used in our previous works. Figure 1 makes explicit the numeration for $g = 0$, 1 and 2. To obtain the new node enumeration at generation $g + 1$, we first squeeze the whole g network into a triangle limited by two outer vertices and the site at the geometrical center of the triangle. The process is completed by adding two identical copies of the squeezed network, rotated by $2\pi/3$ and $4\pi/3$, into the emptied regions. We can verify that, for all values of g, nodes with numbers 1 and 2 are always outer nodes, while the third outer node corresponds to number $N(g)$. The squeezing process always brings the former outer node $N(g)$ to the central position at generation $g + 1$. As a result of the adopted enumeration, we obtain

$$A_2 = \begin{pmatrix} 0 & 1 & 1 & 1 & 1 & 0 & 1 \\ 1 & 0 & 1 & 1 & 0 & 1 & 1 \\ 1 & 1 & 0 & 1 & 0 & 0 & 0 \\ 1 & 1 & 1 & 0 & 1 & 1 & 1 \\ 1 & 0 & 0 & 1 & 0 & 0 & 1 \\ 0 & 1 & 0 & 1 & 0 & 0 & 1 \\ 1 & 1 & 0 & 1 & 1 & 1 & 0 \end{pmatrix}. \tag{1}$$

3. DTQW operators

3.1. Linear chain and the Hadamard coin operator

For the sake of a better understanding of our AN model formulation, we think it is wise to consider the simpler DTQW on an infinite linear chain. Here, we consider a spin-1/2 particle that can be located in any of the available sites and, at each given discrete time interval τ, it

first changes its spin state and, just after, jumps either to the right or to the left. The particle motion is embedded in a Hilbert space $\mathcal{H} = \mathcal{H}_\infty \otimes \mathcal{H}_2$, where $\mathcal{H}_2$ denotes the spin component space. The particle's state is described by a (state) vector $|\Psi\rangle = |\Phi(i)\rangle \otimes |\sigma(\tau)\rangle$, with position $|\Phi\rangle$ and spin $|\sigma\rangle$ components. Both components depend on the node position i and discrete time $n\tau \to n$. It is convenient to write $|\sigma\rangle = \alpha_+|0\rangle + \alpha_-|1\rangle$, where $|0\rangle$ and $|1\rangle$ indicate, respectively, the $\pm 1/2$ spin eigenstates. α_+ and α_- are the magnitudes of each spin eigenstate in the state vector, which are also related to the jump (or shift) dynamics.

At a given value of τ, the time evolution operator $\hat{W}$ acts on $|\Psi(i, n)\rangle$ to produce a new $|\Psi(i, n+1)\rangle$ state in a twofold way: (i) in the first step, a flip (or coin) operator $\hat{C}$ changes the current state of the spin component; (ii) in the second step, the shift operator $\hat{S}$, which depends on the spin state, changes the current probability of finding the particle along the chain sites. In general, it is possible to write $\hat{W} = \hat{S}(\hat{I_\infty} \otimes \hat{C})$. The choice of the flip operator $\hat{C}$ defines the model. For two state spin variables, it is possible to consider a generalization of the Hadamard operator $\hat{H}$ defined either by its action on eigenstates ($\hat{H}|0\rangle = [\cos\theta|0\rangle + \sin\theta|1\rangle]$, $\hat{H}|1\rangle = [\sin\theta|0\rangle - \cos\theta|1\rangle]$) or by its matrix representation

$$\hat{H} = \begin{pmatrix} \cos\theta & \sin\theta \\ \sin\theta & -\cos\theta \end{pmatrix}, \tag{2}$$

where the standard value is $\theta = \pi/4$. If we consider the eigenstates $|i\rangle$ of the position operator $\hat{i}$, i.e. $\hat{i}|i\rangle = i|i\rangle$, the shift operator can be written as

$$\hat{S} = \left[\sum_{i=-\infty}^{\infty} |i+1\rangle\langle i|\right] |0\rangle\langle 0| + \left[\sum_{i=-\infty}^{\infty} |i-1\rangle\langle i|\right] |1\rangle\langle 1|. \tag{3}$$

As shown in [4] , the equivalence between CTQW and DTQW in a chain can be achieved in the limit $\tau \to \infty$, $\theta \to \pi/2$ and $\cos\theta\tau \to 2\gamma t$, where γ is the hopping probability and t is the continuous time in the CTQW formalism. Equations (2) and (3) (or their suitable versions) appear quite frequently in most of the works on DTQW. Here, we want to go a step further and write down the matrix representation of the operator $\hat{W}$ as

$$\hat{W} = \begin{pmatrix} \ddots & \vdots & \vdots & \vdots & \vdots & \vdots & \vdots & \\ \cdots & 0 & 0 & 0 & 0 & 0 & 0 & \cdots \\ \cdots & 0 & 0 & s & -c & 0 & 0 & \cdots \\ \cdots & c & s & 0 & 0 & 0 & 0 & \cdots \\ \cdots & 0 & 0 & 0 & 0 & s & -c & \cdots \\ \cdots & 0 & 0 & c & s & 0 & 0 & \cdots \\ \cdots & 0 & 0 & 0 & 0 & 0 & 0 & \cdots \\ & \vdots & \vdots & \vdots & \vdots & \vdots & \vdots & \ddots \end{pmatrix}, \tag{4}$$

where we explicitly write down the matrix elements corresponding to two spin eigenstates ($|0\rangle$, $|1\rangle$) of three sites in the sequence ($x = -1, 0, 1$): $|-1\rangle|0\rangle$, $|-1\rangle|1\rangle$, ..., $|1\rangle|1\rangle$. c and s are abbreviations for $\cos\theta$ and $\sin\theta$, respectively.

The matrix representation of the DTQW time evolution operator $\hat{W}$ ought to be compared to its CTQW counterpart, which consists of the simple tri-diagonal matrix t, the elements of which can be expressed in term of Kronecker's symbol δ_{ij} as $t_{ij} = \delta_{i,j-1} + \delta_{i,j+1}$. Note that, in contrast to the CTQW tri-diagonal matrix, W in (4) is not symmetric.

3.2. ANs and the Fourier coin operator

We now focus our attention on the DTQW time evolution operator $\hat{W}_g$ for g-dependent ANs. A comparison between this task and the corresponding one for the linear chain shows that the

main difference is the presence of nodes with the different degree k_i. In a given generation g, the possible values of k for AN nodes are $3 \times 2^{g-\ell}$, with $\ell = 1, \ldots, g$. The only exceptions are the three outmost (or corner) nodes with the degree $k_o = 2^g + 1$. In order to keep the same basic DTQW features used for the linear chain, and write down an operator $\hat{W}$ according to the general structure as in (4), the value of k must be equal to the number of spin states in the corresponding node. In a similar fashion, the local coin operator $\hat{C}$ must be defined on a Hilbert space of dimension k.

The degree heterogeneity prevents the presentation of a simple form for the $\hat{S}$ operator as that in (3), not only by the different number of spin components in each node, but also because it is necessary to prescribe locally the precise way the walker moves according to the coin operator output. Since $k \geqslant 3$, it is no longer possible to define them in terms of jumps to the right or to the left as in the previous model, so we think it is wiser to present a matrix representation of $\hat{W}_g$ operator in a similar way as that in (4). As a matter of fact, all results we obtained for $g \leqslant 4$ were based on the actual construction of such matrix representations.

Let us consider the so-called Fourier operator $\hat{F}$ [27], which has been successfully used when one wants to define a DTQW on square lattices as well as in a linear chain where, at each value of τ, the walker also has a choice of remaining in the same node. In the last situation, the local coin operator is presented with the following matrix representation:

$$\hat{F} = \frac{1}{\sqrt{3}} \begin{pmatrix} 1 & 1 & 1 \\ 1 & a & b \\ 1 & b & a \end{pmatrix}, \tag{5}$$

with $a = (-1 + \mathrm{i}\sqrt{3})/2 = b^{-1}$. The respective coin states are denoted by $|0\rangle, |1\rangle$ and $|2\rangle$. The operator $\hat{F}$ can be generalized in a straightforward way to construct the local coin operators for the AN nodes with different degrees. So, let us consider the following matrix representation:

$$\hat{F}(k) = \frac{1}{\sqrt{k}} \begin{pmatrix} 1 & 1 & 1 & \cdots & 1 \\ 1 & \omega_k & \omega_k^2 & \cdots & \omega_k^{(k-1)} \\ 1 & \omega_k^2 & \omega_k^4 & \cdots & \omega_k^{2(k-1)} \\ \vdots & \vdots & \vdots & \cdots & \vdots \\ 1 & \omega_k^{(k-1)} & \omega_k^{2(k-1)} & \cdots & \omega_k^{(k-1)^2} \end{pmatrix}, \tag{6}$$

where $\omega_k = \mathrm{e}^{2\pi \mathrm{i}/k}$ is a primitive kth root of unity, $k = 3 \times 2^\ell$, $\ell = 1, 2, \ldots, g$, or $k = 2^g + 1$. For $k = 3$, (6) reduces to (5). We denote by $|\sigma\rangle$, $\sigma = 0, 1, \ldots, k-1$, the k spin eigenstates in a site with k neighbors.

For $g = 1$, all four nodes have the same degree $k = 3$. The factor in $\hat{W}$ that plays the role of $(\hat{I}_\infty \otimes \hat{C})$ for the linear chain corresponds to the external product of the 4×4 identity matrix $\hat{I}_4$ by the $\hat{F}$ representation (5). The shift operator $\hat{S}$ is represented by the matrix A_1 (just the first four lines and columns in equation (1)) in a two-step procedure: (i) replace each element $(A_1)_{ii}$ by a 3×3 block of 0s; (ii) replace $(A_1)_{ij}$, with $i \neq j$, by a 3×3 block, with the information of which coin state allows the walker to jump from node j to node i. For instance, if the block $(A_1)_{12}$ is represented by a 3×3 matrix, with the $(3, 3)$ element set to 1 while all other elements are set to 0, the walker moves from node 2 to node 1 when the coin state $|2\rangle$ is selected.

As the association of the coin state to the walker movement is arbitrary, we considered the following aspects in our choice: (i) all neighbors of a given node have equal probability of being chosen; (ii) the walker should not go back to the node it came from by the same

coin outcome. The first aspect is equivalent to choosing $\theta = \pi/4$ in (3), while the second just reproduces the fact that, in the chain, left and right moves are always associated with different coin states. This leads to the $\hat{S}_1$ representation

$$\hat{S}_1 = \begin{pmatrix} 0&0&0&0&0&0&0&0&0&1&0&0\\ 0&0&0&0&0&0&0&1&0&0&0&0\\ 0&0&0&0&0&1&0&0&0&0&0&0\\ 1&0&0&0&0&0&0&0&0&0&0&0\\ 0&0&0&0&0&0&0&0&0&0&1&0\\ 0&0&0&0&0&0&0&0&1&0&0&0\\ 0&0&0&1&0&0&0&0&0&0&0&0\\ 0&1&0&0&0&0&0&0&0&0&0&0\\ 0&0&0&0&0&0&0&0&0&0&0&1\\ 0&0&0&0&0&0&1&0&0&0&0&0\\ 0&0&0&0&1&0&0&0&0&0&0&0\\ 0&0&1&0&0&0&0&0&0&0&0&0 \end{pmatrix}. \tag{7}$$

Finally, by performing the matrix multiplication of (7) by $\hat{I}_4 \otimes \hat{F}$, we obtain

$$\hat{W}_1 = \frac{1}{\sqrt{3}} \begin{pmatrix} 0&0&0&0&0&0&0&0&0&1&1&1\\ 0&0&0&0&0&0&1&a&b&0&0&0\\ 0&0&0&1&b&a&0&0&0&0&0&0\\ 1&1&1&0&0&0&0&0&0&0&0&0\\ 0&0&0&0&0&0&0&0&0&1&a&b\\ 0&0&0&0&0&0&1&b&a&0&0&0\\ 0&0&0&1&1&1&0&0&0&0&0&0\\ 1&a&b&0&0&0&0&0&0&0&0&0\\ 0&0&0&0&0&0&0&0&0&1&b&a\\ 0&0&0&0&0&0&1&1&1&0&0&0\\ 0&0&0&1&a&b&0&0&0&0&0&0\\ 1&b&a&0&0&0&0&0&0&0&0&0 \end{pmatrix}, \tag{8}$$

where $a = b^{-1} = \omega_3$ has been defined after equation (5).

The $g = 2$ matrix representation of $\hat{W}_2$ has 30 lines and columns, resulting from the addition of the individual dimensions of the local coin operators. Since each of them must be equal to an individual node degree, we take into account three nodes with $k = 3$, three nodes with $k = 5$ and one node with $k = 6$. Just as in the previous case, each matrix element $(A_2)_{ij}$ of (1) is replaced by a $k_i \times k_j$ block. All blocks in the main diagonal have only zeros. Since it is not possible to represent it in a regular print paper, we indicate below the block structure for the $\hat{W}_2$ operator representation:

$$\hat{W}_2 = \begin{pmatrix} 0^{5,5} & B_{12}^{5,5} & B_{13}^{5,3} & B_{14}^{5,6} & B_{15}^{5,3} & 0^{5,3} & B_{17}^{5,5} \\ B_{21}^{5,5} & 0^{5,5} & B_{23}^{5,3} & B_{24}^{5,6} & 0^{5,3} & B_{26}^{5,3} & B_{27}^{5,5} \\ B_{31}^{3,5} & B_{32}^{3,5} & 0^{3,3} & B_{34}^{3,6} & 0^{3,3} & 0^{3,3} & 0^{3,5} \\ B_{41}^{6,5} & B_{42}^{6,5} & B_{43}^{6,3} & 0^{6,6} & B_{45}^{6,3} & B_{46}^{6,3} & 4_{47}^{6,5} \\ B_{51}^{3,5} & 0^{3,5} & 0^{3,3} & B_{54}^{3,6} & 0^{3,3} & 0^{3,3} & B_{57}^{3,5} \\ 0^{3,5} & B_{62}^{3,5} & 0^{3,3} & B_{64}^{3,6} & 0^{3,3} & 0^{3,3} & B_{67}^{3,5} \\ B_{71}^{5,5} & B_{72}^{5,5} & 0^{5,3} & B_{74}^{5,6} & B_{75}^{5,3} & B_{76}^{5,3} & 0^{5,5} \end{pmatrix}. \tag{9}$$

In the above matrix, the superscripts note the dimension of each indicated block, while blocks composed only by vanishing matrix elements are indicated by $0^{k_i,k_j}$. While the ANs at

generations $g = 3$ and 4 have 16 and 43 nodes, the matrix representations of the operators $\hat{W}_3$ and $\hat{W}_4$ have dimensions 84 and 246, respectively.

3.3. General forms of coin operator

The DTQW evolution depends both on the wavefunction at $T = 0$ and on the coin operator for which the only requirement is that it must satisfy the unitary property. Both the Hadamard and Fourier operators that have been mostly used in DTQW studies satisfy this property. However, other different operators can and have been used in the study of DTQW on regular lattices (see [29]). For the sake of presenting a more complete picture of the problem we analyze, let us briefly discuss the difficulties and consequences of other coin operator choices for the DTQW on ANs.

As detailed and discussed in [28], the general form of unitary operators U_n on an n-dimensional vector space can be expressed in terms of $n(n-1)/2$ *angle* and $n(n+1)/2$ *phase* variables. As the case of the dimension of the W operators just illustrated in the previous subsection, the presence of nodes with a different degree in the AN for $g > 1$ also causes the number of available parameters in the unitary operators to grow exponentially with g. Because of this, it is impossible to address this question for general values of g in a single work. Therefore, we will limit ourselves to the discussion of the situations in which $n = 2$ (linear chain) and $n = 3$ ($g = 1$ AN).

For the first case, the most general form of U_2 can be written as

$$U_2 = \begin{pmatrix} c\mathrm{e}^{\mathrm{i}\alpha_1} & s\mathrm{e}^{\mathrm{i}\alpha_2} \\ -s\mathrm{e}^{\mathrm{i}(\alpha_1-\alpha_2+\alpha_3)} & c\mathrm{e}^{\mathrm{i}\alpha_3} \end{pmatrix}, \tag{10}$$

indicating that the Hadamard operator (2) corresponds to the choice $\alpha_1 = \alpha_2 = 0$ and $\alpha_3 = \pi$.

When $n = 3$, it is usual to represent U_3 as a product of simpler matrices. In such a case, three angles $\theta_i (i = 1, 2, 3)$, and six phases $\alpha_i (i = 1, \ldots, 6)$ are combined according to

$$\begin{aligned} U_3 = &\begin{pmatrix} 1 & 0 & 0 \\ 0 & \mathrm{e}^{\mathrm{i}\alpha_1} & 0 \\ 0 & 0 & \mathrm{e}^{\mathrm{i}\alpha_2} \end{pmatrix} \begin{pmatrix} 1 & 0 & 0 \\ 0 & 1 & 0 \\ 0 & 0 & \mathrm{e}^{-\mathrm{i}\alpha_6} \end{pmatrix} \begin{pmatrix} 1 & 0 & 0 \\ 0 & c_1 & s_1 \\ 0 & -s_1 & c_1 \end{pmatrix} \begin{pmatrix} 1 & 0 & 0 \\ 0 & 1 & 0 \\ 0 & 0 & \mathrm{e}^{\mathrm{i}\alpha_6} \end{pmatrix} \\ &\times \begin{pmatrix} c_2 & s_2 & 0 \\ -s_2 & c_2 & 0 \\ 0 & 0 & 1 \end{pmatrix} \begin{pmatrix} 1 & 0 & 0 \\ 0 & c_3 & s_3 \\ 0 & -s_3 & c_3 \end{pmatrix} \begin{pmatrix} \mathrm{e}^{\mathrm{i}\alpha_3} & 0 & 0 \\ 0 & \mathrm{e}^{\mathrm{i}\alpha_4} & 0 \\ 0 & 0 & \mathrm{e}^{\mathrm{i}\alpha_5} \end{pmatrix}. \end{aligned} \tag{11}$$

The Fourier coin is obtained for the phases $\alpha_1 = \alpha_3 = \alpha_4 = \alpha_5 = 0$, $\alpha_2 = \alpha_6 = 3\pi/2$, and $c_1 = 1/\sqrt{3}$, $s_1 = \sqrt{2}/\sqrt{3}$ and $c_2 = s_2 = -c_3 = s_3 = 1/\sqrt{2}$. For the purpose of illustrating the effect of other coin operators, in the next section we will explore results for the Fourier coin as well as for the following uniform values of phases and angles in (11): $\alpha_j = 0$, and (a) $\theta_i = \pi/4$, (b) $\theta_i = \pi/8$ and (c) $\theta_i = \pi/100$, $\forall i, j$.

4. Results

In this section, we present results for the DTQW time evolution obtained by the successive application of the operator $\hat{W}_g$ to an initial state $|\Psi_0\rangle$ that depends both on the position of the walker $|\Phi_0\rangle$ and the coin state $\hat{C}$. We have worked mainly with two distinct choices for the walker position: the walker has probability 1 of being in the central node $j = c$, or the walker can be found with equal probability in any of the nodes. In the first case, as j refers to the central node, the corresponding state is denoted by $|\Phi_0\rangle = |\Phi_{c,0}\rangle$, while the equal probability condition is indicated by $|\Phi_0\rangle = |\Phi_{e,0}\rangle$. While the coin states have been chosen according to similar rules to those used for the linear chain, the explicitly used rules can be inferred from

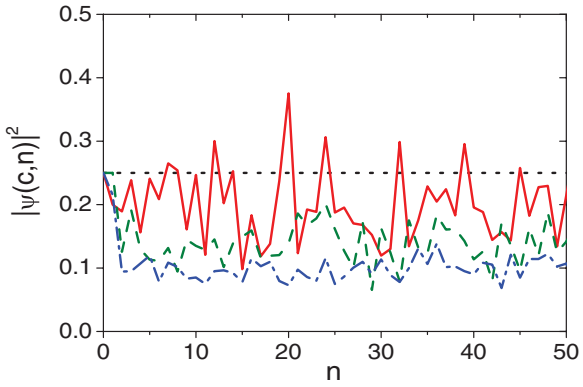

Figure 2. Time evolution of $|\Psi(i = c, n)|^2$ for $g = 1, 2, 3$ and 4 indicated, respectively, by (black) dots, solid (red) line, (green) dashes and (blue) dash dots. The same initial condition $|\Phi_0(i)| = |\Psi(i, n = 0)| = 1/\sqrt{N(g)}$ is valid for all generations. For this particular initial condition, the time-independent solution for all nodes at $g = 1$ is also observed for other choices of angles and phases in the coin operator.

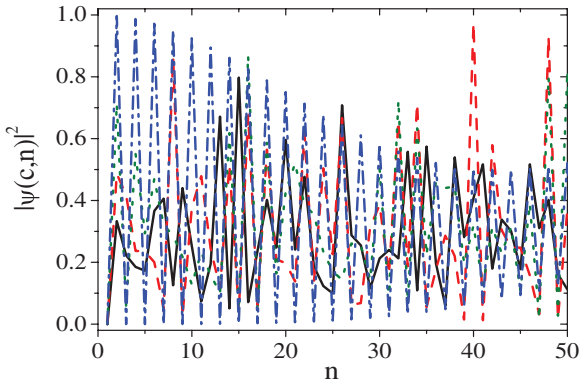

Figure 3. Time evolution of $|\Psi(i = c, n)|^2$ for $g = 1$ and the Fourier coin (black solid line) and different choices of $\theta_i = \pi/4$ (red dashes), $\theta_i = \pi/8$ (green dots) and $\theta_i = \pi/100$ (blue dash-dots). The initial condition is $|\Phi_0\rangle = |\Phi_{c,0}\rangle$. In the last three cases, $\alpha_j = 0\ \forall j$. The curves illustrate the dependence of the coin operator C. If compared to figure 2, it also shows the sensibility to the initial condition $|\Phi_0\rangle$.

the form of the $\hat{W}_g$ matrix representations. As anticipated above, we use the coin operator (6) for all $g > 1$.

4.1. Time evolution of the probability distribution

We show in figure 2 the probability of finding the walker in the central node as a function of time when $|\Phi_0\rangle = |\Phi_{0,e}\rangle$ (solid symbols and lines). When $g = 1$, all four nodes are equivalent, so that $|\Psi(i, n)|^2 = 1/4$, $\forall i, n$ (black dashes in figure 2). For $g > 1$, this property no longer holds. The curves clearly indicate that $|\Psi(i = c, n)|^2$ depends on time in a rather complex way. The curves for $|\Psi(i, n)|^2$, $i \neq c$, also have a similar and irregular behavior.

An irregular behavior is the characteristic feature for the $|\Phi_{0,c}\rangle$ initial condition. In such a case, even the dynamics for the $g = 1$ network become irregular. This is illustrated in figure 3, where we show how the probability of finding the walker in the central node depends on

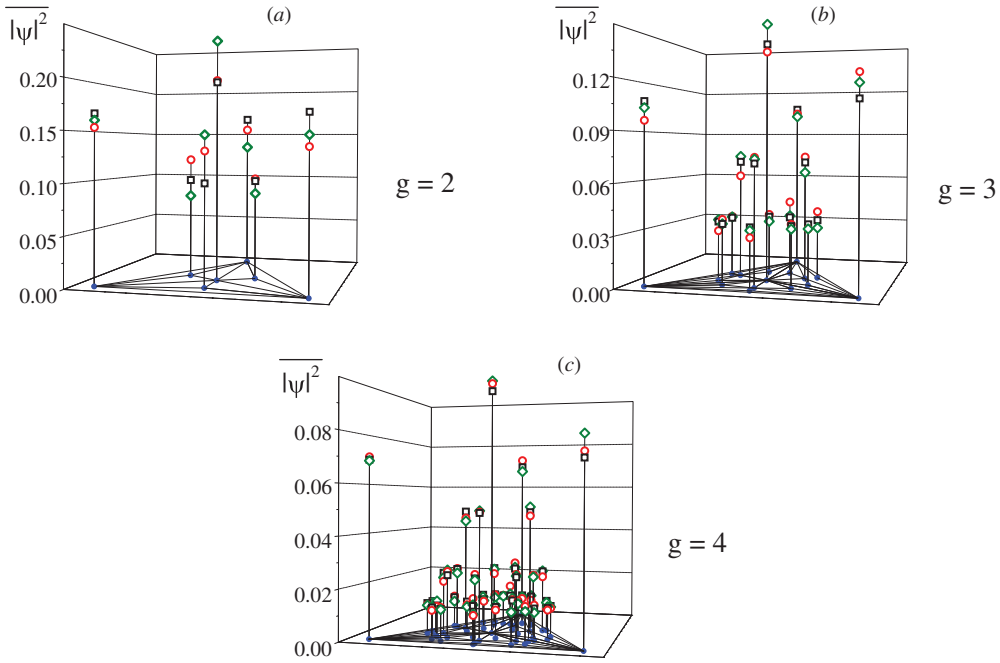

Figure 4. Time average $\overline{|\Psi(i)|^2}$ for $g = 2$, 3 and 4 and two distinct initial conditions: $|\Phi_0\rangle = |\Phi_{0,e}\rangle$ (red) circles $|\Phi_0\rangle = |\Phi_{0,c}\rangle$ (green) diamonds. Black squares correspond to the asymptotic occupation probability of a classical walk, which is independent of the initial conditions. Total time is $T = 10\,000$.

time when $|\Phi_0\rangle = |\Phi_{c,0}\rangle$. For the purpose of emphasizing the dependence on the coin state, we draw the values of $|\Psi(i = c, n)|^2$ for different choices of the coin operator indicated in the previous section. Quite irregular behavior is the common feature for all but the choice $\alpha_j = 0, \theta_i = \pi/100, \forall i, j$. In the last case, the time evolution is characterized by a sinusoidal long period oscillation superimposed onto high-frequency changes between small and large values of $|\Psi(i = c, n)|^2$.

4.2. Time-averaged probability distribution

We have next evaluated the time average

$$\overline{|\Psi(i)|^2} = \lim_{T\to\infty} \frac{1}{T} \sum_{n=1}^{T} |\Psi(i, n)|^2 \tag{12}$$

as a function of the node i and different initial conditions. The results in figure 4 for $g = 2, 3$, reproduce the results for two different initial conditions: $|\Phi_{0,e}\rangle$ and $|\Phi_{0,c}\rangle$.

It is quite clear that the possible values of $\overline{|\Psi(i)|^2}$ are distributed close to discrete horizontal planes that go through the admitted normalized values $\overline{k_i} = k_i/\sum_\ell k_\ell$, indicating that the probability of finding the walker in a given node i is strongly correlated with k_i, and hence the generation in which it was introduced into the network. Keeping in mind that the corresponding exact result for the classical DTRW on AN is $\overline{k_i}$, irrespective of the initial condition, we look for the following signatures of DTQW behavior: (i) differences among nodes with the same k for a given initial condition; (ii) differences among the results for one same node as a function of the initial conditions. Both features are clearly displayed in figures 4(*a*) and (*b*), when $g = 2$

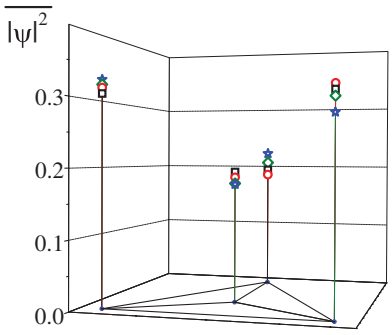

Figure 5. Time average $\overline{|\Psi(i)|^2}$ for $g = 1$ and the Fourier coin (black squares) and different choices of $\theta_i = \pi/4$ (red circles), $\theta_i = \pi/8$ (green diamonds) and $\theta_i = \pi/100$ (blue stars). The initial condition is $|\Phi_0\rangle = |\Phi_{c,0}\rangle$. Total time is $T = 10\,000$. The average probability presents slightly large memory coin dependence.

and 3. When $g = 4$, such differences become small in comparison to the differences in the values of k, as one notes from figure 4(*c*).

In figure 5, we illustrate the dependence of $\overline{|\Psi(i)|^2}$ on the choice of the coin operator when $g = 1$. In such a case, we consider $|\Phi_0\rangle = |\Phi_{0,c}\rangle$ and make use of the Fourier coin and three further angle choices indicated in the previous section. The results clearly indicate the dependence on the choice of parameters defining the unitary transformation. We call attention to the fact that, for all four operators, we use the same form of the $\hat{S}_1$ matrix in equation (7).

4.3. Time transition probability distribution from the central node

Now let us consider the quantum transition probability $\pi_{i,j}$ for a walker to go from node j to node i in n time steps as a function of the initial conditions. This requires that the initial condition be expressed by $|\Phi_{0,j}\rangle = |j\rangle$ or $|\Phi_{0,j}(i)|^2 = \delta_{i,j}$.

Results are shown in figure 6. The upper panel illustrates the behavior of $\pi_{i,j}$ for all sites ($i = 1, 2, 3, 4$) of the first generation, when $j = c = 3$ corresponds to the central node (see figure 1). We draw the results for the Fourier coin only. $\pi_{i,j} = |\Psi(i)|^2$ has a quite different behavior as compared to that for the homogeneous initial conditions in figure 2. Although each of the four nodes has the same degree $k = 3$, the time evolution depends on the site, as a consequence of the influence of the coin state on the movement. As we have already observed in figures 3 and 5, the choice of other coin operators leads to distinct values $\pi_{i,j}(n)$.

In the lower panel of figure 6 we illustrate a typical behavior for $g = 4$. We again take the central node as an initial condition, which now amounts to taking the state $|\Phi_{0,16}\rangle$. We show values of $\pi_{i,j}$ for selected nodes with $k = 2^4 + 1$ and $k = 3 \times 2^{4-i}$, with $i = 1, 2, 3, 4$. They correspond, respectively, to nodes introduced into the network at generations $g = 0, 1, 2, 3$ and 4. The time dependence shows similar oscillations to those already present in the $g = 1$ case. It is also interesting to note that the values of $\pi_{i,j}$ fluctuate around the few plateaus $\overline{k_i}$ that define the obtained probability values for the classical DTRW.

4.4. Comparison between DTQW and CTQW

It is important to stress important differences between DTQW and CTQW results for ANs [23]. Since the CTQW evolution operator is essentially expressed by $\exp(\mathrm{i}Ht)$, where the uniform tight binding Hamiltonian H coincides with the AN adjacency matrix, it is represented by a

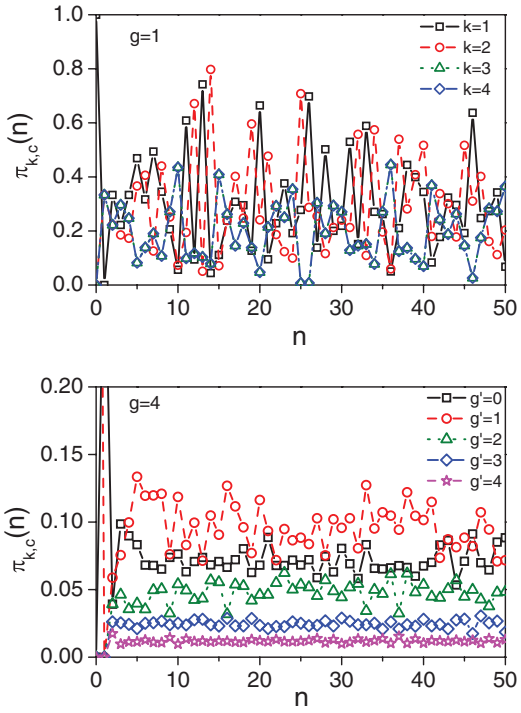

Figure 6. Quantum transition probability $\pi_{i,j}(n)$ for a walker to go from node $j = c$ to node i in n steps. For $g = 1$, the transition probabilities for all four nodes are shown. Due to the coin used and the choice $j = c = 3$, the values of $\pi_{3,3}(n)$ and $\pi_{4,3}(n)$ coincide for all values of n. The same does not happen to $\pi_{1,3}(n)$ and $\pi_{2,3}(n)$. For $g = 4$, we draw $\pi_{i,16}(n)$ for five different nodes introduced at, respectively, generations $g' = 0$, 1, 2, 3, and 4. As g' increases, the nodes have a smaller number of neighbors and smaller probability of hosting the walker.

periodic series involving the eigenvalues of H. When $g = 1$, all eigenvalues can be analytically evaluated [11], so that the authors have obtained an exact expression for the periodic transition probabilities $\pi_{i,j}$. For larger values of g, the ratio between any two eigenvalues of H is no longer a rational number. As a consequence, $\pi_{i,j}(\forall(i, j))$ are no longer periodic, but they still follow a smooth path. In contrast, figures 2 and 6 clearly show quite irregular oscillations for all values of g. This behavior results from the successive multiplication of the operator $\hat{W}_g$ on the initial state. As the eigenvalues of $\hat{W}_g$ are distinct from those of H already when $g = 1$, it is natural to obtain distinct results for DTQW and CTQW. Another striking difference between the two results is the order of magnitude of $\pi_{i,j}$ as the function of k. While our results are characterized by irregular oscillations around values that are roughly proportional to $\overline{k_i}$, CTQW values vary in a much more drastic way (see figure 2 of [23]). This leads, for instance, to rather a localized state when the initial condition is located on the central node, in a marked difference to our results.

5. Conclusions

In this work, we reported results for the DTQW on Apollonian networks of up to 43 sites. We developed a framework leading to the construction of an explicit matrix representation of the

time evolution operator $\hat{W}_g$, which takes into account the actions of the coin and displacement operators. This way, the discrete time evolution was achieved by successively multiplying the time evolution matrix by the state vector describing the walker state at a previous discrete time. Since the node degree is non-uniform, it was necessary to consider Fourier coin operators acting locally in spaces with a dimension given by the specific node degree.

We have shown that the time evolution of the walker state is very sensitive to initial conditions and to the choice of action of the coin operators. This becomes quite explicit in the analysis of $g = 1$ AN, where different probabilities (walker state components) are obtained for sites that are geometrically equivalent.

The results we presented for the time-dependent behavior and asymptotic averages are quite distinct in comparison to those for CTQW on the same ANs. This supports the current view resulting from investigations in regular lattices that the discrete and continuous time quantum walks represent quite distinct dynamical processes.

As briefly mentioned in the introduction, the equivalence between DTQW and CTWR is only achieved under some limiting conditions on the coin operator, which depend on the dimensionality of the lattice and other topological properties. Different approaches have been worked out in this direction [4–6] but, for the current problem, it is necessary to take into account that the coin operator depends on the node the walker visits acting. This rules out the simpler proposals developed in the first two references quoted above. Further work may resolve the derivation of the proper limit conditions for the mapping from DTQW to CTQW.

Acknowledgments

The authors acknowledge the financial support of the Brazilian agencies FAPESB (project PRONEX 0006/2009) and CNPq. Both authors also acknowledge the National Institute of Science and Technology for Complex Systems.

References

[1] Aharonov Y, Davidovich L and Zagury N 1993 *Phys. Rev.* A **48** 1687
[2] Farhi E and Gutmann S 1998 *Phys. Rev.* A **58** 915
[3] Mulken O and Blumen A 2011 *Phys. Rep.* **502** 37
[4] Strauch F W 2006 *Phys. Rev.* A **74** 030301
[5] D'Alessandro D 2010 *Rep. Math. Phys.* **66** 85
[6] Childs A 2010 *Commun. Math. Phys.* **294** 581
[7] Andrade J S Jr, Herrmann H J, Andrade R F S and da Silva L R 2005 *Phys. Rev. Lett.* **94** 018702
[8] Vieira A P, Andrade J S Jr, Herrmann H J and Andrade R F S 2007 *Phys. Rev.* E **76** 026111
[9] Kaplan C N, Hinczewski M and Berker A N 2009 *Phys. Rev.* E **79** 061120
[10] Araujo N A M, Andrade R F S and Herrmann H J 2010 *Phys. Rev.* E **82** 046109
[11] Andrade R F S and Miranda J G V 2005 *Physica* A **356** 1
[12] Souza A M C and Herrmann H J 2007 *Phys. Rev.* B **75** 054412
[13] Cardoso A L, Andrade R F S and Souza A M C 2008 *Phys. Rev.* B **78** 214202
[14] de Oliveira I N, de Moura F A B F, Lyra M L, Andrade J S Jr and Albuquerque E L 2009 *Phys. Rev.* E **79** 016104
[15] Newman M E J, Barabási A-L and Watts D J 2006 *The Structure and Dynamics of Networks* (Princeton, NJ: Princeton University Press)
[16] Boccaletti S, Latora V, Moreno Y, Chavez M and Hwang D-U 2006 *Phys. Rep.* **424** 175
[17] Costa L F, Rodrigues F A, Travieso G and Villas Boas P R 2007 *Adv. Phys.* **56** 167
[18] Barabasi A L and Albert R 1999 *Science* **286** 509
[19] Watts D J and Strogatz S H 1998 *Nature* **393** 440
[20] Albert R and Barabasi A-L 2002 *Rev. Mod. Phys.* **74** 47
[21] Dorogovtsev S N, Goltsev A V, Mendes J F F and Samukhin A N 2003 *Phys. Rev.* E **68** 046109

[22] Giuraniuc C V, Hatchett J P L, Indekeu J O, Leone M, Perez Castillo I, Van Schaeybroeck B and Vanderzande C 2006 *Phys. Rev.* E **74** 036108
[23] Xu X-P, Li W and Liu F 2008 *Phys. Rev.* E **78** 052103
[24] Zhang Z, Guan J, Xie W, Qi Y and Zhou S 2009 *Europhys. Lett.* **86** 10006
[25] Cirac J I, Ekert A K, Huelga S F and Macchiavello C 1999 *Phys. Rev.* A **59** 4249
[26] Raussendorf R and Briegel H J 2001 *Phys. Rev. Lett.* **86** 5188
[27] Oliveira A C, Portugal R and Donangelo R 2006 *Phys. Rev.* A **74** 012312
[28] Rašin A 1997 arXiv:hep-ph/9708216v1
[29] Tregenna B, Flanagan W, Maile R and Kendon V 2003 *New J. Phys.* **5** 83